JJMIE

Volume 2, Number 2, Jun. 2008
ISSN 1995-6665
Pages 101 - 109

Jordan Journal of Mechanical and Industrial Engineering

Analytical Approximate Solution for Decaying Laminar Swirling Flows within A Narrow Annulus

Ali M. Jawarneh [a]*, Georgios H. Vatistas [b], and Amer Ababneh [a]

[a] Department of Mechanical Engineering, The Hashemite University, Zarqa 13115, Jordan
[b] Department of Mechanical and Industrial Engineering, Concordia University, 1455 de-Maisonneuve Blvd.West, Montreal, Canada

Abstract

Analytical solutions of the Navier-Stokes equations for laminar fully developed flow in a cylindrical annulus for decaying swirling flows have been derived for narrow- gap geometry. Expressions are derived for axial and swirl velocities, as well as for the pressure. Generally, the swirl velocity exhibits a Hagen-Poiseuille flow profiles and these profiles decay gradually downstream because of wall friction, which leads to damp the tangential velocity. For flows with small gap, the swirl velocity will develop faster than a wider gap where the tangential velocity curves start flatter mid-gap and any further increases in axial position, the decaying of swirl velocity will develop rapidly. When the Reynolds number increases the tangential velocity, profile flattens mid-gap. The dimensionless pressure is non-linear and it is very sensitive to inlet swirl and Reynolds numbers. It decreases downstream exponentially and steeper for small gap. The comparison between analytical and predicted results shows good agreement in overall trends. A good correlation between the present analytical model and numerical results is evident as the maximum difference between them is less than 5%.

Keywords: Swirling Flows; Narrow Annulus; Vortex Decay;

Nomenclature

B_n	Fourier-Bessel constant
L	length of the two cylinders
P	pressure
P_o	reference pressure
$\Delta\bar{P}$	dimensionless pressure
r_i	radius of the inner cylinder
r_o	radius of the outer cylinder
r, θ, z	components of the location in the cylindrical co-ordinates
$\bar{r}$	dimensionless radius
R_e	Reynolds number
R_E	reduced Reynolds number
S	inlet swirl number
V, U	axial and tangential inlet velocity components
V_z, V_φ	axial and tangential velocity components
$\bar{V}_z, \bar{V}_\varphi$	dimensionless axial and tangential velocity components
$\bar{z}$	dimensionless axial position

Greek Symbols

α	gap ratio
β	constant
ν	kinematic viscosity
μ	dynamic viscosity
ρ	density

1. Introduction

The flow in cylindrical annuli, which has been widely utilized in boiler, feed water heaters, heat exchangers, extruders, cooling the rotor and stator of motors and generators has been investigated extensively. The use of decaying swirl flow is one of most promising techniques for enhancing the momentum and heat transfer. The presence of swirl will increase the flow path, decrease the free area and introduce an angular acceleration to the fluid flow [1-2]. Swirling flows can be imparted to the flow by use of various swirl-generating methods [3-7] where part of fluid enters axially while the reminder is injected tangentially using a vortex generator. References 3 and 4 discussed the flow field for a cylindrical vortex flow, while the present work-study the flow between two concentric cylinders. Vortex decay flow is the major key connection between references three and four and the present work.

Mateescu and Paidoussis [8] have studied the effect of swirl in axial flow through a narrow gap. When the fluid

* Corresponding author. e-mail: jawarneh@hu.edu.jo

gap is, narrow both fluid viscosity and inertia effects are of importance. Analytical solution for laminar, fully developed flow due to impose oscillating pressure gradient in annulus was studied by Tsangaris [9]. The fully developed laminar flow of a generalized Newtonian fluid through annuli was analyzed by Escudier et al [10], with a power-law viscosity function. The effects of eccentricity and inner-cylinder rotation were also studied. The characteristics of turbulent swirling flow in axisymmetric annuli using the particle image velocimetry (PIV) technique has been studied by Chang [11]. Farias et al [12] have performed numerical study to estimate the hydrodynamics of an annular swirling decaying flow induced by means of a single tangential inlet in laminar flow regime. The mean swirl intensity in the completely annular gap thickness has been found to decrease from the entrance section.

A simple exact solution of the laminar velocity field between two concentric rotating cylinders (Schlichting [13]) is well known where the axial and radial velocity components are zero while the azimuthal is function of radial cylindrical coordinate. It is well known that Taylor [14], first considered the stability of a viscous flow in a small annular gap between concentric cylinders with rotation of the inner one, called Taylor-Couette flow. He found experimentally and theoretically that the flow is stable when both cylinders are stationary and when the inner cylinder is stationary while the outer one is rotating for laminar flow. Therefore, the exact solution in this paper is valid because the two cylinders are stationary and the flow is laminar.

Many researchers have studied the instability causing Taylor vortices [15-17]. All laminar flows are subjected to instability. Therefore, the exact solution in this paper is valid only for a certain finite range of the Reynolds numbers.

In decaying vortex flow, the methodology of calculating the velocity components and pressure profiles in the flow between two stationary cylinders is quite limited in the open literature. Therefore, this paper concerns an analytical study of laminar fully developed flow of an incompressible viscous fluid confined between two stationary cylinders with small gap. The fluid is enforced to flow downstream by an imposed swirl and axial velocity components at the entrance. The fluid is adverted downstream due to an axial pressure gradient but also subjected to centrifugal mechanisms due to imposed swirl at the entrance. The coexistence of centrifugal and an axial flow mechanism within the gap will be studied. A numerical simulation will also be employed in this study to compare with the exact solution.

2. Mathematical Formulation

We consider an incompressible fluid of dynamic viscosity μ and density ρ contained between two long stationary concentric cylinders whose inner and outer radii are r_i and r_o, respectively. Fig. shows the schematic of the annulus and co-ordinates system. The fluid enters the cylinders gap uniformly with two velocity components (V, U) in z, θ directions, where V and U denote the axial and tangential inlet velocity components, respectively. The equations will be solved for a steady, laminar, axisymmetric and incompressible flow, and assuming that the gap between the two cylinders is very small, and the radial velocity is also assumed to be zero since it doesn't have the space and time to develop.

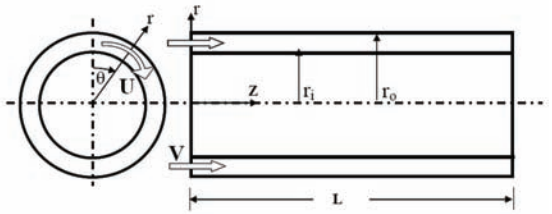

Fig.1: Swirling flow between two concentric cylinders

The velocity (V_z ,V_φ) and pressure P are governed by the continuity and Navier-Stokes equations as

$$\frac{\partial V_z}{\partial z} = 0 \qquad (1)$$

$$\frac{\partial P}{\partial r} = \rho \frac{V_\varphi^2}{r} \qquad (2)$$

$$-\frac{\partial P}{\partial z} + \mu\left(\frac{d^2 V_z}{dr^2} + \frac{1}{r}\frac{dV_z}{dr}\right) = 0 \qquad (3)$$

$$\rho V_z \frac{\partial V_\varphi}{\partial z} = \mu\left(\frac{\partial^2 V_\varphi}{\partial r^2} + \frac{1}{r}\frac{\partial V_\varphi}{\partial r} - \frac{V_\varphi}{r^2}\right) \qquad (4)$$

where V_z and V_φ denote the axial velocity and swirl velocity components. Eq. (1) indicates that V_z does not change in the flow direction, i.e., V_z is independent of z or $V_z \neq f_n(z)$. The flow can be considered fully developed since the two cylinders are sufficiently long so that entry and exit effects can be neglected. Equation (2) suggests that the centrifugal force on an element of fluid balances the force produced by the radial pressure gradient.

We define non-dimensional quantities as follows:

$$\bar{V}_z = \frac{V_z}{V}, \bar{V}_\varphi = \frac{V_\varphi}{U}, S = \frac{U}{V}, \bar{z} = \frac{z}{L},$$
$$\bar{r} = \frac{r}{r_i}, \alpha = \frac{r_o}{r_i}, \Delta\bar{P} = \frac{\Delta P}{\rho V^2} \qquad (5)$$
$$\Delta P = P - P_o, \; R_e = \frac{r_i V}{\nu}, \quad R_E = R_e\left(\frac{r_i}{L}\right)$$

where S, L, α, P_o, ν, R_e and R_E are the inlet swirl number, which measures the ratio of the rate of the injected tangential momentum flux to the rate of axial momentum flux, the length of two cylinders, the gap ratio, the pressure at a reference point, the kinematic viscosity of the fluid, the Reynolds number and the reduced Reynolds number, respectively.

Introduce the above parameters into the continuity and momentum equations. Thus, we get:

$$\frac{\partial \bar{V}_z}{\partial \bar{z}} = 0 \quad or \quad \bar{V}_z = f_n(\bar{r}) \qquad (6)$$

$$\frac{\partial \Delta\bar{P}}{\partial \bar{r}} = S^2 \frac{\bar{V}_\varphi^2}{\bar{r}} \qquad (7)$$

$$\frac{d^2\bar{V}_z}{d\bar{r}^2}+\frac{1}{\bar{r}}\frac{d\bar{V}_z}{d\bar{r}}=R_E\frac{\partial\Delta\bar{P}}{\partial\bar{z}} \quad (8)$$

$$\bar{V}_z\frac{\partial\bar{V}_\varphi}{\partial\bar{z}}=\frac{1}{R_E}\left(\frac{\partial^2\bar{V}_\varphi}{\partial\bar{r}^2}+\frac{1}{\bar{r}}\frac{\partial\bar{V}_\varphi}{\partial\bar{r}}-\frac{\bar{V}_\varphi}{\bar{r}^2}\right) \quad (9)$$

The last equation can be linearzed by assuming the non-dimensional axial velocity $\bar{V}_z\approx 1$. This linear methodology can be justified for many reasons. First, many authors have used it as an example see [18]. Second, since the non-dimensional axial profile is fully developed (parabolic profile), it means that the dimensionless axial profile change only in the radial direction, so Eq.(9) will be solved approximately by taking the bulk or mean effect of the dimensionless axial velocity profile which is 1. Third, in any standard fluid textbook, the axial velocity profile in pipe flow can be evaluated as a uniform velocity by including the kinetic-energy correction factor, the kinetic-energy correction factor is considered to have a constant value. Finally, if the present approximation is not valid this means that the analytical solution and the numerical results for the tangential (swirl) velocity will not match, but later if you see the comparison you will see how much these profiles are matching well.

By linearizing the non-dimensional axial velocity $\bar{V}_z\approx 1$ in the last non-linear differential equation, since the non-dimensional axial velocity is fully developed, the θ-momentum equation is reduced to:

$$\frac{\partial\bar{V}_\varphi}{\partial\bar{z}}\cong\frac{1}{R_E}\left(\frac{\partial^2\bar{V}_\varphi}{\partial\bar{r}^2}+\frac{1}{\bar{r}}\frac{\partial\bar{V}_\varphi}{\partial\bar{r}}-\frac{\bar{V}_\varphi}{\bar{r}^2}\right) \quad (10)$$

One method of obtaining the solution to solve the last partial differential equation is the method of separation variables. This method assumes that $\bar{V}_\varphi(\bar{z},\bar{r})$ is written as a product as follows:

$$\bar{V}_\varphi=\psi(\bar{z})\,\Phi(\bar{r}) \quad (11)$$

Substitute back in Eq.(10), we get two ordinary differential equations. The first one has the following form:

$$\frac{d\psi}{d\bar{z}}+\frac{\lambda^2}{R_E}\psi=0 \quad (12)$$

in addition, its solution is:

$$\psi(\bar{z})=c_o\exp\left[-\frac{\lambda^2}{R_E}\bar{z}\right] \quad (13)$$

where c_o is constant.

The second equation is second order differential equation has the following form:

$$\frac{d^2\Phi}{d\bar{r}^2}+\frac{1}{\bar{r}}\frac{d\Phi}{d\bar{r}}+\left[\lambda^2-\frac{1}{\bar{r}^2}\right]\Phi=0 \quad (14)$$

The general solution of the differential Eq. (14) can be expressed in terms of Bessel functions

$$\Phi(\bar{r})=AJ_1(\lambda\bar{r})+BY_1(\lambda\bar{r}) \quad (15)$$

where $J_1(\lambda\bar{r})$ is known as the Bessel function of the first kind of order 1, $Y_1(\lambda\bar{r})$ is known as the Bessel function of the second kind of order 1, A and B are constants. Let the constant c_o in Eq. (13) equal to one, then $\bar{V}_\theta$ becomes:

$$\bar{V}_\varphi=\{AJ_1(\lambda\bar{r})+BY_1(\lambda\bar{r})\}\exp\left[-\frac{\lambda^2}{R_E}\bar{z}\right] \quad (16)$$

Applying the boundary conditions to the solution:

(i) $\bar{r}=1$, $\bar{V}_\varphi=0$

these boundary conditions give:

$$A=-B\frac{Y_1(\lambda)}{J_1(\lambda)}$$

(ii) $\bar{r}=\frac{r_o}{r_i}=\alpha$, $\bar{V}_\varphi=0$

from this boundary condition, we must take $B\neq 0$ since otherwise $\bar{V}_\varphi=0$. The set of Bessel functions $J_1(\lambda_n\bar{r}), Y_1(\lambda_n\bar{r})$, n=0, 1, 2, …, are orthogonal with respect to the weight function of $\bar{r}$ when the eigenvalues λ_n are defined by means of a boundary condition (ii) of the form

$$Y_1(\lambda_n\alpha)J_1(\lambda_n)-Y_1(\lambda_n)J_1(\lambda_n\alpha)=0 \quad (17)$$

Equation (16) becomes:

$$\bar{V}_{\varphi n}=B_n\left\{-\frac{Y_1(\lambda_n)}{J_1(\lambda_n)}J_1(\lambda_n\bar{r})+Y_1(\lambda_n\bar{r})\right\}\exp\left[-\frac{\lambda_n{}^2}{R_E}\bar{z}\right] \quad (18)$$

By using the appropriate boundary conditions:

(iii) $\bar{z}=0$, $\bar{V}_\varphi=1$

these boundary conditions give:

$$1=B_n\left\{Y_1(\lambda_n\bar{r})-\frac{Y_1(\lambda_n)}{J_1(\lambda_n)}J_1(\lambda_n\bar{r})\right\} \quad (19)$$

Using the orthogonal of the eignfunctions, one obtains an expression for the Fourier-Bessel constant B_n as:

$$B_n=\frac{\int_1^\infty\left\{(\lambda_n\bar{r})-\frac{Y_1(\lambda_n)}{J_1(\lambda_n)}J_1(\lambda_n\bar{r})\right\}\bar{r}\,d\bar{r}}{\int_1^\infty\left\{(\lambda_n\bar{r})-\frac{Y_1(\lambda_n)}{J_1(\lambda_n)}J_1(\lambda_n\bar{r})\right\}^2\bar{r}\,d\bar{r}} \quad (20)$$

The first 40 values of B_n are presented in Table 1 for a gap ratio α of 1.2. These values are sufficient to calculate the swirl velocity with an error of less than 0.1 percent.

Finally, the solution of tangential velocity can be written as:

$$\bar{V}_\varphi=\sum_{n=0}^{\infty}B_n\left\{-\frac{Y_1(\lambda_n)}{J_1(\lambda_n)}J_1(\lambda_n\bar{r})+Y_1(\lambda_n\bar{r})\right\}\exp\left[-\frac{\lambda_n{}^2}{R_E}\bar{z}\right] \quad (21)$$

In order to get an explicit expression for the pressure that appears in Eq.[7], an approximation of Bessel functions for large arguments can be written as:

$$J_1(\lambda_n \bar{r}) \approx \sqrt{\frac{2}{\pi \lambda_n \bar{r}}} \cos(\lambda_n \bar{r} - \frac{3\pi}{4}) \quad (22)$$

$$Y_1(\lambda_n \bar{r}) \approx \sqrt{\frac{2}{\pi \lambda_n \bar{r}}} \sin(\lambda_n \bar{r} - \frac{3\pi}{4}) \quad (23)$$

Let:

$\eta_n = \lambda_n \bar{r} - \frac{3\pi}{4}$, $a_n = \tan(\lambda_n - \frac{3\pi}{4})$

Table 1: Important eigenvalues and Fourier-Bessel constants

n	λ_n	B_n	n	λ_n	B_n
0	15.7277	4.48076	20	329.868	1.02034
1	31.4259	0.498397	21	345.576	0.04541
2	47.1305	2.66573	22	361.284	0.975147
3	62.8368	0.10547	23	376.992	0.043484
4	78.5438	2.0771	24	392.7	0.935471
5	94.2511	0.086467	25	408.408	0.041784
6	109.959	1.7599	26	424.116	0.900274
7	125.666	0.07503	27	439.824	0.040269
8	141.374	1.55426	28	455.532	0.868773
9	157.082	0.067187	29	471.24	0.038908
10	172.789	1.40713	30	486.948	0.840363
11	188.497	0.06138	31	502.655	0.037676
12	204.205	1.29516	32	518.363	0.814569
13	219.913	0.056858	33	534.071	0.036554
14	235.621	1.20628	34	549.779	0.791013
15	251.329	0.053207	35	565.487	0.035527
16	267.037	1.13349	36	581.195	0.76939
17	282.744	0.05018	37	596.903	0.034581
18	298.452	1.07246	38	612.611	0.749448
19	314.16	0.047617	39	628.319	0.033708

then the r-momentum, Eq. (7), can be simplified as:

$$\Delta\bar{P}(\bar{r},\bar{z}) = S^2 \int \frac{\bar{V}_\varphi^2}{\bar{r}} d\bar{r} + f(\bar{z}) \quad (24)$$

or

$$\Delta\bar{P}(\bar{r},\bar{z}) \approx \frac{2S^2}{\pi} \sum_{i=0}^{\infty}\sum_{j=0}^{\infty} \frac{B_i B_j}{\sqrt{\lambda_i \lambda_j}} \exp\{-\frac{2\bar{z}(\lambda_i^2+\lambda_j^2)}{R_E}\} \int (\sin\eta_i - a_i\cos\eta_i)(\sin\eta_j - a_j\cos\eta_j)\frac{1}{\bar{r}^2} d\bar{r} + f(\bar{z}) \quad (25)$$

Derive the last equation with respect to $\bar{z}$ yields:

$$\frac{\partial\Delta\bar{P}(\bar{r},\bar{z})}{\partial\bar{z}} \approx \frac{4S^2}{\pi R_E} \sum_{i=0}^{\infty}\sum_{j=0}^{\infty} B_i B_j \left(-\frac{(\lambda_i^2+\lambda_j^2)}{\sqrt{\lambda_i\lambda_j}}\right) \exp\{-\frac{2\bar{z}(\lambda_i^2+\lambda_j^2)}{R_E}\} \int (\sin\eta_i - a_i\cos\eta_i)(\sin\eta_j - a_j\cos\eta_j)\frac{1}{\bar{r}^2} d\bar{r} + \frac{df(\bar{z})}{d\bar{z}} \quad (26)$$

We know from Eq.(21) that the maximum swirl velocity or the centrifugal force occurs at the mid-gap location $\Re = \frac{1}{2}(\alpha+1)$ of the annular because the previous experiments showed that the maximum swirl velocity occurs at the mid-gap, please see [19-21]. This means that the centrifugal force dominates the flow at this location. Therefore, if we evaluate Eq. (26) at $\Re$ and equate it with z-momentum, Eq. (8), we get

$$\frac{d^2\bar{V}_z}{d\bar{r}^2} + \frac{1}{\bar{r}}\frac{d\bar{V}_z}{d\bar{r}} \approx R_E \frac{d\Delta\bar{P}(\bar{r}=\Re,\bar{z})}{d\bar{z}} \quad (27)$$

The last equation shows that the left hand side is a function of $\bar{r}$ while the right hand side is a function of $\bar{z}$. Therefore, the two functions must be equal to constant. Let the constant to be β then Eq.(27) becomes

$$\frac{d^2\bar{V}_z}{d\bar{r}^2} + \frac{1}{\bar{r}}\frac{d\bar{V}_z}{d\bar{r}} = \beta \quad (28)$$

The solution of Eq.(28) is:

$$\bar{V}_z = \frac{\beta}{4}\bar{r}^2 + c_1 \ln\bar{r} + c_2 \quad (29)$$

Therefore, the axial velocity profile is a parabola and involves three constants, β, c_1 and c_2, which are determined by applying appropriate boundary conditions and the integral form of the continuity equation.

Boundary conditions

(i) $\bar{r} = 1$, $\bar{V}_z = 0$

Therefore, the constant c_2 is solved to be equal:

$$c_2 = -\frac{\beta}{4}$$

(ii) $\bar{r} = \alpha$, $\bar{V}_z = 0$

Therefore, the constant c_1 is solved to be equal:

$$c_1 = \frac{\beta}{4\ln\alpha}\left(1-\alpha^2\right)$$

Substitute the constants c_1 and c_2 back to Eq. (29) yields

$$\bar{V}_z = \frac{\beta}{4}\left[\bar{r}^2 - \left(\alpha^2-1\right)\frac{\ln\bar{r}}{\ln\alpha} - 1\right] \quad (30)$$

From the global continuity, we have:

$$V\pi\left(r_o^2 - r_i^2\right) = \int_{r_i}^{r_o} \frac{\beta}{4} V\left[\bar{r}^2 - \left(\alpha^2-1\right)\frac{\ln\bar{r}}{\ln\alpha} - 1\right] 2\pi r dr$$

in dimensionless form:

$$\alpha^2 - 1 = \frac{\beta}{2}\int_1^{\alpha}\left[\bar{r}^2 - \left(\alpha^2-1\right)\frac{\ln\bar{r}}{\ln\alpha} - 1\right]\bar{r}\, d\bar{r}$$

$$or\ \beta = \frac{8\ln\alpha}{\alpha^2[1-\ln\alpha] - \ln\alpha - 1}$$

The general form of non-dimensional axial velocity can be written as:

$$\bar{V}_z = \frac{2\ln\alpha}{\alpha^2[1-\ln\alpha] - \ln\alpha - 1}\left[\bar{r}^2 - \left(\alpha^2-1\right)\frac{\ln\bar{r}}{\ln\alpha} - 1\right] \quad (31)$$

If Eq. (31) has been inserted back in Eq.(9) the solution may be not possible but the beauty of this work is to obtain the swirl velocity first with valid assumption (average effect of axial velocity) then the pressure, and finally the axial velocity will be solved. Therefore, Eq. (31) is valid simply because it is based on conservation laws (Eq. 8 and Eq. 26), and the agreement between the analytical work and the numerical methodology will approve the validity of these equations.

3. Numerical Method

The above equations are verified by solving numerically the system of full Navier-Stokes and continuity equations using Fluent 6.1 (Fluent INC., 2003) which is a CFD package based on a finite volume method. The problem is considered incompressible, steady, axisymmetric, laminar swirling flow. In this case, we can model the fluid in 2-D (i.e., solve the axisymmetric swirl problem) and incorporate the prediction of the swirl velocity.

The SIMPLE algorithm was used, in order to handle the coupling between pressure and velocity. The second order upwind schemes were used for momentum and first order upwind scheme was used for swirl velocity. For all the simulations performed in this study, converged solutions were usually achieved with residuals as low as 10^{-6} for all governing equations. The 2-D axisymmetric case with 150000 quadrilateral grid cells is chosen and an unstructured grid was used for the present simulation. The mesh is sufficiently refined in order to resolve the expected large flow parameter gradients. The under-relaxation parameters on the velocities were selected 0.3-0.5 for the radial and axial, and 0.9 for the swirl velocity components. Segregated, implicit solver, which is well suited for the sharp pressure and velocity gradients, has been applied through annulus. When using the present laminar model it is necessary to run the simulation for a significant number of iterations, beyond normal convergence criteria. Experience has shown that typically 3000 iterations needed before the peak tangential velocity in the simulation stabilizes. In order to ensure the accuracy of the results and their independence with respect to the number of nodes used in the discretization process, several grids were tested. A grid independent solution study was made by performing the simulations for three different grids consisting of 155031, 150000, and 145000 nodes.

At the inlet to the annulus a uniform velocity components were used. At the outlet boundary there is no information about the variables and some assumptions have to be made. The diffusion fluxes in the direction normal to the exit plane are assumed zero. The pressure at the outlet boundary is calculated from the assumption that radial velocity at the exit is neglected, so that the pressure gradient from r-momentum is given by

$$\frac{\partial P}{\partial r} = \frac{\rho V_{\varphi}^2}{r} \qquad (32)$$

At the solids walls, the no-slip condition was applied where the velocities at the walls were specified to be zero. The centerline boundary was considered axis of symmetry. The working fluid was air at reduced Reynolds number (R_E) of 185 and with an inlet swirl number (s) of 1.67. The gap ratio α set to be 1.2.

4. Analysis of Results

The Results for some representative combinations of the governing parameters were presented and discussed in this study. The solutions were carried out for flows of different inlet swirl number S, reduced Reynolds number R_E and gap ratio α. In addition, the velocity and pressure distributions were derived at various axial and radial positions in the annulus. First, typical dimensionless axial velocity profiles for the fully developed annulus were shown in Figs. 2(a) and 2(b) for gap ratios α =1.2 and 1.4, respectively. The axial velocity profile exhibited a Poiseuille-like profile and independent of the reduced Reynolds and inlet swirl number. The axial velocity obtained numerically for gap ratio α =1.2 was in excellent agreement with the exact solution.

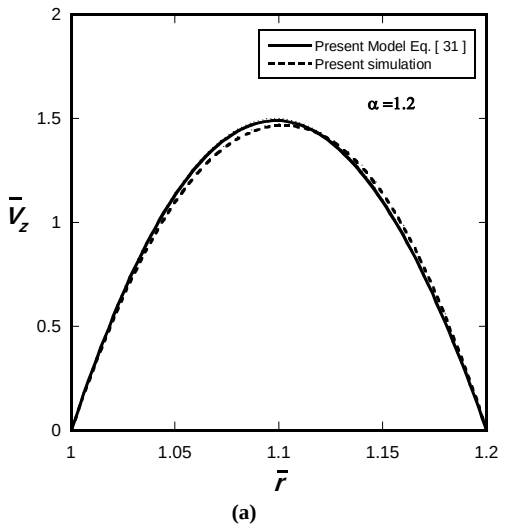

(a)

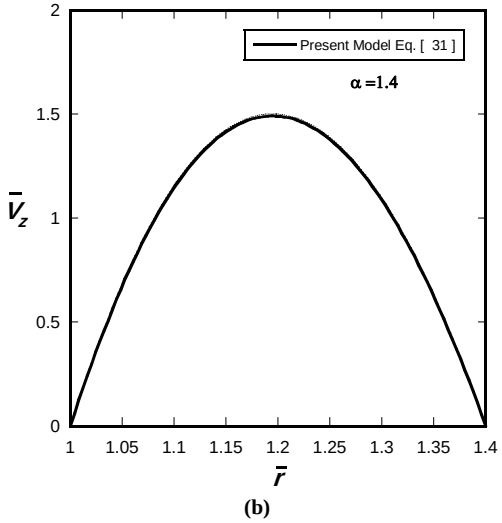

(b)

Fig. 2: Dimensionless axial velocity profile: (a) gap ratio α = 1.2; (b) gap ratio α = 1.4

Fig. 3 shows the development of the non-dimensional swirl velocity in the annulus at different axial positions $\bar{z}$=0.3, 0.5 and 0.8. Generally, at specified reduced Reynolds number, as an example R_E of 185, the swirl velocity exhibits parabolic profiles and these profiles decay downstream because of wall friction, which leads to damp the tangential velocity. All selected profiles at gap ratio α =1.2 are parabolic-like shape as seen from Fig. 3(a). This is well known for flows with small gap that will develop rapidly, but this is not proper for gap ratio α =1.4 at axial location of $\bar{z}$ =0.3 as seen from Fig. 3(b) where the tangential velocity curves start flatter mid-gap and any further increases in axial position, the decaying swirl velocity will develop rapidly. The comparison between analytical and predicted results for the swirl velocity profiles at R_E =185 and α =1.2 shows good agreement in overall trends.

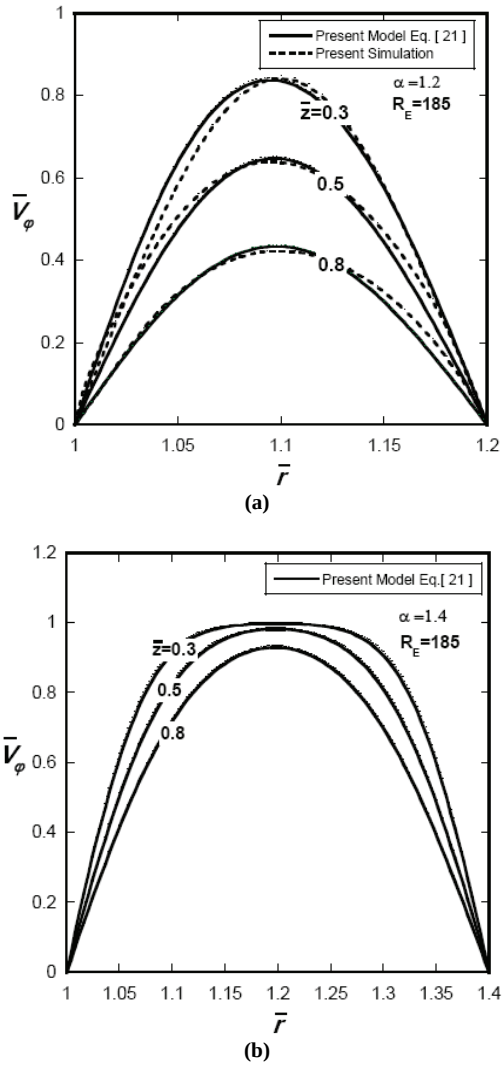

Fig. 3: Dimensionless swirl velocity profiles at reduced Reynolds number R_E =185 for different axial locations: (a) gap ratio α = 1.2; (b) gap ratio α = 1.4

It is evident from Fig. 4 that the tangential velocity distribution is strongly depends on the reduced Reynolds number R_E. If the $\bar{z}$ is specified, say at the mid annulus length, for all range of the reduced Reynolds numbers at small gap ratio α =1.2 the swirl velocity exhibits a Hagen-Poiseuille flow profiles as shown in Fig. 4(a). For gap ratio α =1.4 at low reduced Reynolds numbers R_E the velocity profile exhibits also a Hagen-Poiseuille flow profile, but when R_E increases, the tangential velocity profile flattens mid-gap and progressively spreading towards the walls, where the tangential velocity is seen to reduce to zero within a thin layer, see Fig. 4(b). As an example at high Reynolds number, R_E= 300, where the inertia dominates the viscous effects, the flow in the central region of the annulus behaves as a plug-flow. The comparison between analytical and simulated results for the maximum dimensionless swirl velocity profile at R_E =185 and α =1.2 matches well.

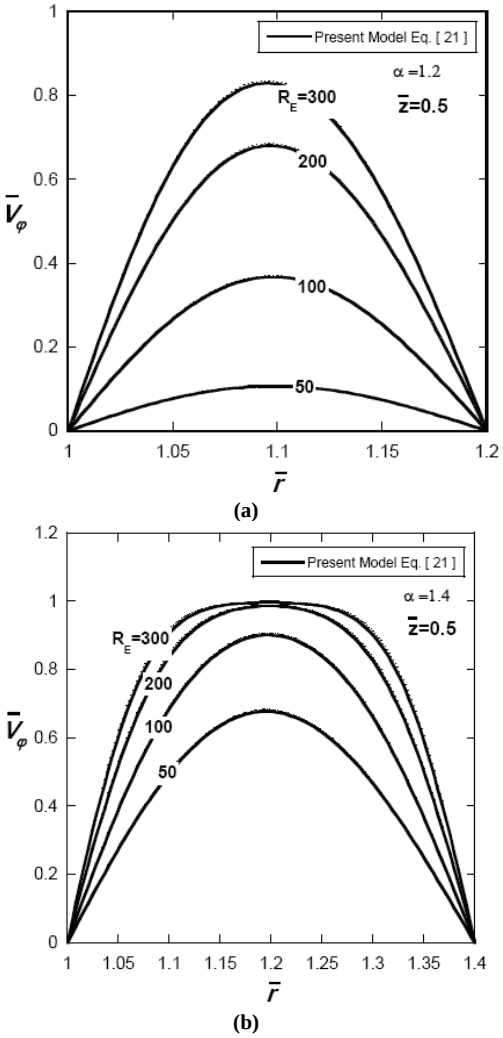

Fig. 4: Dimensionless swirl velocity profiles at axial location $\bar{z}$ = 0.5 for different reduced Reynolds numbers R_E: (a) gap ratio α = 1.2; (b) gap ratio α = 1.4

The maximum tangential velocity, as shown from previous figures, occurs at the mid-gap $\Re = \frac{1}{2}(\alpha+1)$. From Eq. (21), the maximum tangential velocity can be easily determined as

$$\bar{V}_{\varphi\max} = \sum_{n=0}^{\infty} B_n \left\{ -\frac{Y_1(\lambda_n)}{J_1(\lambda_n)} J_1(\lambda_n \Re) + Y_1(\lambda_n \Re) \right\} \exp\left[-\frac{\lambda_n^2}{R_E} \bar{z} \right] \qquad (33)$$

Its variations with different reduced Reynolds numbers R_E are presented in Fig. 5. The peak tangential velocity decreases with the axial distance from the injection location because of the swirl decay. At low reduced Reynolds numbers, the viscous force overshadows the inertia force which suppresses the centrifugal effects, when the flow approaches the annulus exit, as an example at R_E=50 and gap ratio α =1.2 as seen from Fig. 5(a), the flow behaves like a pipe flow or its axially-dominated flow regime. Despite of decaying the vortex, the swirl velocity does not vanish for the gap ratio α =1.4 at low reduced Reynolds number, as seen in Fig. 5(b). This is because the no-slip boundary condition has less effect in a wider gap. An increase of reduced Reynolds number R_E, say R_E=500 for α =1.4, the vortex maintains its strength without a significant decaying along the annulus.

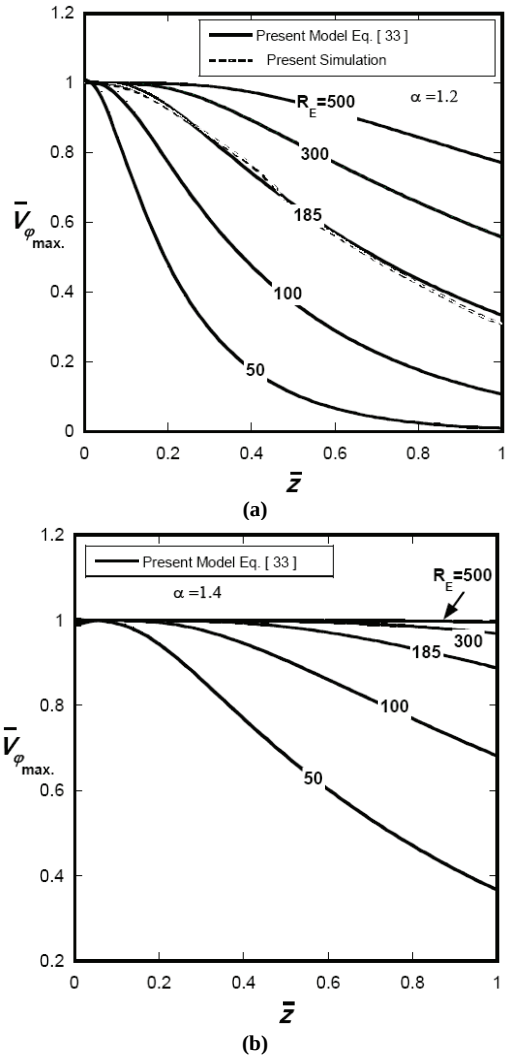

Fig. 5: Maximum dimensionless swirl velocity profiles for different reduced Reynolds numbers R_E: (a) gap ratio α = 1.2; (b) gap ratio α = 1.4

The distribution of the static pressure can be evaluated by substituting the non-dimensional tangential velocity, Eq. (21), in the radial momentum equation, Eq. (24), and by integrating from 1 to α to represent the average effect of the centrifugal force across any section. Therefore, the dimensionless pressure as a function of $\bar{z}$ are written as:

$$\Delta \bar{P}(\bar{z}) \approx \frac{2S^2}{\pi} \sum_{i=0}^{\infty} \sum_{j=0}^{\infty} \frac{B_i B_j}{\sqrt{\lambda_i \lambda_j}} \exp\{-\frac{2\bar{z}(\lambda_i^2 + \lambda_j^2)}{R_E}\} \int_1^{\alpha} (\sin\eta_i - a_i \cos\eta_i)(\sin\eta_j - a_j \cos\eta_j) \frac{1}{\bar{r}^2} d\bar{r} \qquad (34)$$

In Couette flows, the pressure was assumed constant while linear in Poiseuille flows. It is obvious from the last equation that the pressure is non-linear. From last equation, the static pressure is very sensitive to inlet swirl and Reynolds numbers. The effects of the two numbers on the dimensionless pressure are presented in Figs. 6 and 7. Firstly, the effect of the reduced Reynolds number will be discussed at inlet swirl number S=1.67 as seen in Fig. 6. It can be seen that the dimensionless pressure decreases downstream exponentially, and for a particular axial position, the dimensionless pressure is higher for higher value of R_E as depicted in Fig. 6. For lower values of R_E =50 and 100, as shown in Fig. 6(a) for gap ration α =1.2, the dimensionless pressure tends to be zero when the flow approaches the exit port.

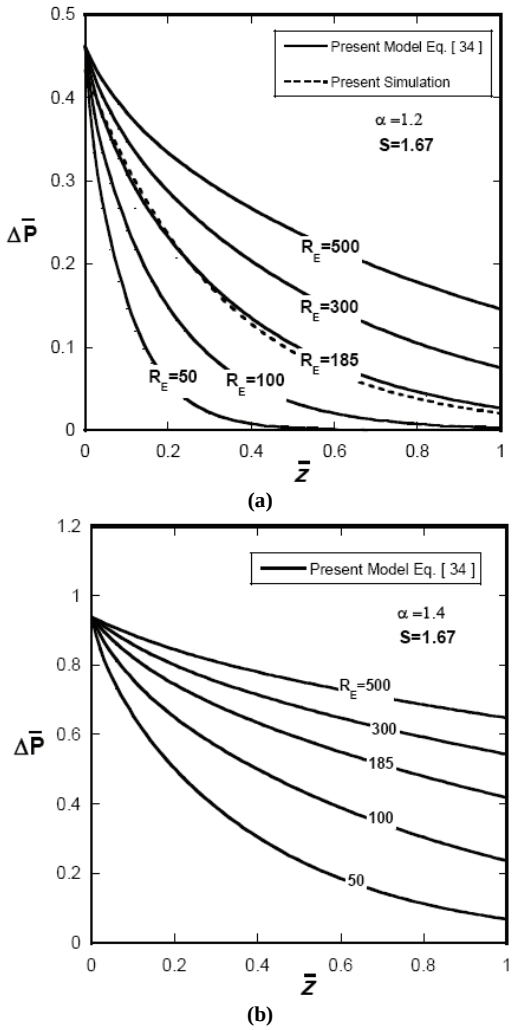

Fig. 6: Dimensionless pressure profiles for different reduced Reynolds numbers R_E: (a) gap ratio α = 1.2; (b) gap ratio α = 1.4

When gap ratio α =1.4, as shown in Fig. 6(b), there is a significant pressure much higher than the case of gap ratio α =1.2. The comparison between analytical and predicted

results for the pressure profile at R_E =185 and α =1.2, as shown in Fig. 6(a), captures well the curve trend. The dimensionless pressure variations for various inlet swirl numbers are presented in Fig. 7. In either (a) or (b) in Fig. 7 the pressure also decreases exponentially with axial location, and for a precise axial position, the dimensionless pressure is higher for higher value of S where the rate of injected tangential momentum flux dominates the rate of axial momentum flux as depicted in Fig. 7.

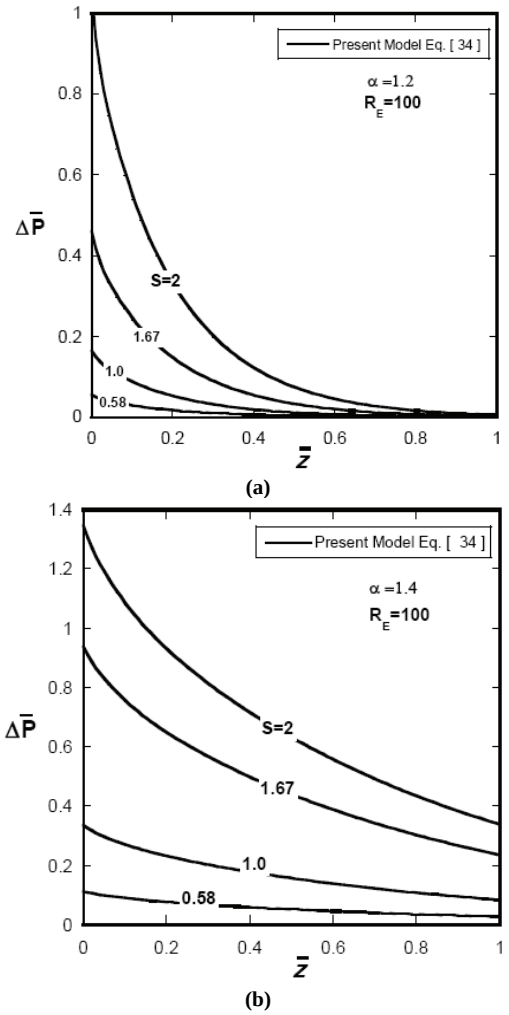

Fig. 7: Dimensionless pressure profiles for different inlet swirl numbers S: (a) gap ratio α = 1.2; (b) gap ratio α = 1.4

A closer consideration however, reveals that in addition to the radial-axial plane flow there is also a substantial centrifugal force, which decays with the length, thus determining the development of the overall flow-field. Dimensionless pressure decreases rapidly for small gap ratio α =1.2, as shown in Fig. 7(a) at R_E=100, and approaches zero at the end of the downstream, while for gap ratio α =1.4 it decreases slowly with considerable pressure values at the end of annulus.

5. Conclusions

Analytical solutions was performed to study the flow field through a laminar cylindrical annulus for decaying swirling flows. Parametric study has been done to observe the effects of Reynolds, inlet swirl numbers and gap ratio on the flow field. The swirl velocity exhibits a Hagen-Poiseuille flow profiles, and these profiles decay gradually downstream because of friction. However, for small gap and/or high Reynolds number, the curves flatters mid-gap. The pressure is non-linear and it is depends on inlet swirl and Reynolds numbers. It decreases downstream exponentially and sharply for small gap. The simulated flow velocities and pressure, solved by means of a finite volume technique, are in a close quantitative agreement with the present analytical results.

References

[1] E.K. Akpinar, Y. Bicer, C. Yildiz, and D. Pehlivan, " Heat Transfer Enhancement in a concentric double pipe exchanger equipped with swirl element". International Communications in Heat and Mass Transfer , Vol. 31, No. 6, 2004, 857-868.

[2] T.H. Kuhen and R.J. Goldstein, "An experimental and theortical study of natural convection in the annulus between horizontal concentric cylinders." Journal of Fluid Mechanics, Vol. 74, 1979, 695-719.

[3] A.M. Jawarneh, P. Sakaris , and G.H. Vatistas, "Experimental and analytical study of the pressure drop across a double-outlet vortex chamber", Transaction of ASME, Journal of Fluids Engineering, Vol. 129, No , 2007, 100-105.

[4] A.M. Jawarneh, G.H. Vatistas and H. Hong, "On the flow development in jet-driven vortex chambers", AIAA, Journal of Propulsion and Power, Vol. 21, No. 3, 2005, 564-570.

[5] Gupta A., Lilley D. G, Swirl Flows,. Abacus Press, Cambridge;1984.

[6] M. Yilmaz, S. Yapici, O. Jomakli, and O.N. Sara, "Energy correlation of heat transfer and enhancement efficiency in decaying swirl flow", Heat Mass Transfer, 38, 2002, 351-358.

[7] R. De Parias Neto, P. Legentilhomme, and J. Legrand, "Finite-element simulation of laminar swirling decaying flow induced by means of a tangential inlet in an annulus", Computer Methods in Applied Mechanics and Engineering, Vol. 165, 1998, 189-213.

[8] D. Mateescu, M.P. Paidoussis, "Unsteady viscous effects on the annular-flow-induced instabilities of a rigid cylinder body in a narrow duct," Journal of Fluid and Structures 1, 1987, 197-215.

[9] Tsangaris, "Oscillatory flow of an incompressible viscous fluid in a straight annulus pipe," Journal de Mecanique Theorique et Appliquee. Vol.3, No.3, 1984, 467-478.

[10] M.P. Escudier, P.J. Oliveira and F.T. Pinho,"Fully developed laminar flow of purely viscous non-Newtonian liquids through annuli, including the effects of eccentricity and inner-cylinder rotation," International Journal Heat Fluid Flow, Vol. 23, 2002, 52-73.

[11] T.H. Chang, "Experimental study on turbulent swirling flow in a cylindrical annuli by using the PIV technique," International Journal of Automotive Technology, Vol. 5, No. 1, 2004, 17−22.

[12] S.R. De Farias Neto, P Legentilhomme, and J. Legrand, " Finite-element simulation of laminar swirling decaying flow induced by means of a tangential inlet in an annulus", Computer Methods In Applied Mechanics And Engineering , Vol. 165, 1998, 189-213.

[13] Hermann Schlichting , Boundary-Layer Theory, 7th edition, McGraw-Hill, Cambridge; 1979.

[14] G.L. Taylor, "stability of a viscous fluid contained between two rotating cylinders," Philos. Trans. R. Soc. London, Ser. A, Vol. 223, 1923, 289-343.

[15] S.T. Wereley and R.M. Lueptow, " spatio-temporal character of non-wavy and wavy Taylor-Couette Flow," Journal of Fluid Mechanics, Vol. 364, 1998, 59-80.
[16] A. Meseguer and F. Marques, " On the competition between centrifugal and shear instability in spiral Couette flow". Journal of Fluid Mechanics,Vol. 402, 2000, 33-56.
[17] I. Donald, Takeuchi, Daniel, and F. Jankowski," A Numerical and experimental investigation of the stability of spiral Poiseuille flow." Journal of Fluid Mechanics, Vol 102., 1981,101-126.
[18] Vatistas G.H., Ghaly W., and Tsifourdaris P. "Swirling Inflow Within the Narrow Gap of Two Disks," Journal Propulsion And Power, Vol. 21, No. 4, 2005, 743-750.
[19] F. Marques, J. M. Lopez, “Taylor Couette flow with axial oscillations of the inner cylinder: Floquet analysis of the basic flow”, Journal of Fluid Mechanics, Vol. 348, 1997, 153-175.
[20] F. Marques, J. Sanches, P. D. Weidman, “Generalized Couette-Poiseuille flow with boundary mass transfer”, Journal of Fluid Mechanics,Vol. 374, 1998, 221-249.
[21] S. Tsangaris , N.W. Vlachakis “Exact solution for the pulsating finite gap Dean flow,” Applied Mathematical Modeling, Vol. 31, 2007, 1899–1906.